JOURNAL OF APPLIED ELECTROCHEMISTRY 23 (1993) 371–378

Potentiostatic passivation of zinc in alkaline solutions

P. L. CABOT, M. CORTES, F. CENTELLAS, E. PEREZ

Departament de Química Física, Facultat de Química, Universitat de Barcelona, Avinguda Diagonal, 647, 08028 Barcelona, Spain

Received 13 February 1992; revised 21 July 1992

The potentiostatic passivation of upward-facing horizontal zinc electrodes in quiescent 0.4–4 M KOH solutions has been studied according to different models and by SEM, coulometry and ICP. An initial flat maximum was found for all the potentiostatic transients except in 0.4 M KOH. The greatest part of the transients consisted in the initial maximum followed by a current plateau and a sigmoidal sharp decrease. The remaining curves were gradual modifications of the latter. The first part of all the transients could be interpreted according to a diffusion-controlled growth of a porous film coupled to metal dissolution from the electrode surface. In this model, the metal is dissolved as its ions and part of them react with the anions already present in the solution to form the anodic film, the rate of electrocrystallization being determined by the instantaneous concentration of the metal ions at the electrode surface. However, the second phenomenon appearing in practically all the potentiostatic transients, i.e., the current plateau and further sigmoidal sharp decrease must be explained by a model of 2D ohmic-controlled film growth.

1. Introduction

The electrochemical behaviour of zinc in alkaline media continues to be a field of considerable importance because of its interest in batteries and its potential application in advanced energy storage devices. The mechanism of zinc dissolution into zincate has been studied previously using the galvanostatic, potentiostatic, potentiodynamic, RDE and impedance techniques [1–8]. Recent work agrees with the mechanism already proposed by Bockris *et al.* [1, 2, 4, 7].

The potentiodynamic curves of zinc in KOH, exemplified in Fig. 1, consist of five regions [4–6, 8–11]: an active dissolution into zincate, in which the current increases exponentially with potential (X), a linear *I–E* region (L), a pseudopassive region, where the current varies slowly with potential (around the maximum M), a sharp decrease in current (P) and a passive region in which the current is almost independent of potential (A), with currents lower than those corresponding to the pseudopassive region.

Under potentiodynamic conditions, mass transport effects have been invoked to explain the deviation of the exponential dependence of current with potential in the anodic dissolution of the metal [4, 7, 9, 10]. Direct optical evidence of a film near the maximum in the potentiodynamic curves has been reported by Powers and Breiter [11]. However, this phase has been suggested to form in the linear *I–E* region, much before the anodic maximum [4, 8, 12, 13], by a dissolution–precipitation process with a significant component of dissolution [4] or by direct formation on the metal surface, the dissolution being the rate determining step [8].

Three main types of metal passivation have been described in the literature: (a) a dissolution–precipitation process [4, 9, 14, 15], (b) an adsorption process [16, 17] and (c) a nucleation and growth process [18, 19]. The first has been invoked to explain galvanostatic and potentiodynamic experiments in the presence, and in the absence, of forced convection, while the solid state routes have been basically suggested from potential-controlled experiments under hydrodynamic conditions (RDE).

Despite the information obtained on the properties of the passive film formed potentiostatically [5, 20–22], the potentiostatic transients corresponding to oxide film growth have not been previously studied. In the present work, potentials corresponding to the prepassive and to the passive region of the potentiodynamic curves have been applied to high-purity zinc in a range of KOH concentrations 0.4–4 M to interpret such potentiostatic transients in quiescent solutions on the light of different models.

2. Experimental details

The experiments were performed at 25.0 ± 0.1 °C using a vertical cell of volume 100 cm^3, the working electrode being upward-facing. As counter and reference electrodes, a platinum mesh and the Hg/HgO/OH^- (C) half cell were employed, respectively, the latter being connected via a Luggin capillary. All the potentials given in this work are referred to such a reference electrode. The working solutions were deaerated 0.4, 1, 2, 3 and 4 M KOH, prepared with Millipore Milli-Q quality water and the Merck p.a. product.

The instrumentation used has been described previously [4], save for the addition to the recorders of a 3091 Nicolet digital storage oscilloscope and a 731

0021-891X

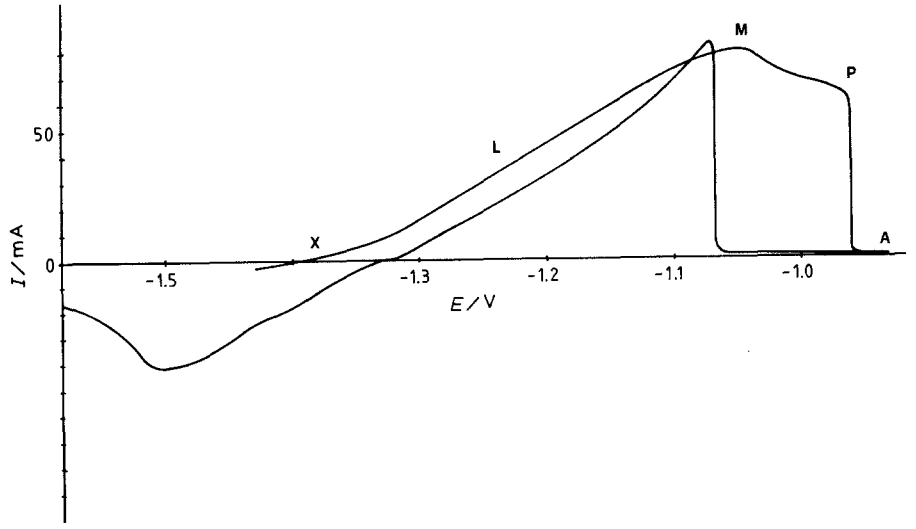

Fig. 1. Cyclic polarization curve of zinc in quiescent 4M KOH solution at $5\,mV\,s^{-1}$.

Amel integrator, the experimental curves being transferred to a LY-1800 *X-Y* Linseis recorder for a further analysis.

The working electrode consisted of an 8 mm diameter cylindrical rod of 99.9% pure zinc (Merck). Only the base of the cylinder was exposed to the electrolyte. After a mechanical polishing up to a mirror finish, the metal was introduced to the cell and electrochemically treated by means of three cyclic polarizations between -1.6 and -0.8 V at a sweep rate of $50\,mV\,s^{-1}$ with forced convection. In addition, a cathodic polarization at -1.425 V also with forced convection was performed for 5 min. The potentiostatic pulse was applied 30 s after stopping the forced convection.

Certain experiments were carried out using zinc (99.9%) discs of 8 mm diameter and 1 mm thickness. These samples were embedded in epoxy resin to present to the medium the upward face of the disc. After the experiment, the sample was immediately removed from the solution and stirred in benzene to eliminate the layer of electrolyte adhering to the surface, thus precluding further precipitations. Afterwards, the samples were dried in an argon atmosphere. A collection of samples were stored under high vacuum to be observed directly under a Jeol-JSM 840 SEM, furnished with a Link Systems EDX. Duplicates of the samples were embedded totally in epoxy resin and further abraded, polished and metallized with a gold film of 10 nm, to observe the film section and the metal roughness. The zinc content of the working solution after the electrolysis was determined by means of a Jobin Yvon JY38VHR inductively coupled argon plasma spectroscope.

3. Results

3.1. *Potentiostatic transients*

The potential range selected for the potentiostatic transients was from -1.2 to -0.7 V, which includes the prepassive and the passive zones of the potentiodynamic curves (see Fig. 1). Certain examples of potentiostatic transients are shown in Fig. 2a–e, where it is easily seen that they depend on the potential applied and the KOH concentration. The different types of potentiostatic curves are shown schematically in Fig. 3. For reasons of simplicity in describing and treating the experimental curves, a code has been associated with each type. The form of the potentiostatic transients found for each potential and KOH concentration is shown in Table 1, where the codes defined in Fig. 3 have been employed. From this Table, the evolution of the potentiostatic curves with potential and concentration is evident. The largest section corresponds to type C_m, consisting of an initial current decrease (*h* in Fig. 3), a maximum (m), a decay (d) followed by a plateau (n) and a further decay with an inflexion point (i). When the applied potential is more positive, the difference between the anodic currents corresponding to the maximum 'm' and to the region 'n' decreases up to a point that the difference is very small (see Fig. 2e).

The unique concentration in which the initial maximum 'm' was not detected was 0.4 M (Table 1). In 1 M KOH, such a maximum was only found for potentials in the range from -1.2 to -1.1 V. In order to elucidate the mechanism of the process, $\log I_m$ was plotted against $\log t_m$, where I_m and t_m are the current and time corresponding to the maximum 'm' in curves S_m, S_{mm}, and C_m (Fig. 4). The slope of such plots were -0.56, -0.54 and -0.56 for 2, 3 and 4 M KOH, respectively.

The current corresponding to the minimum c (see Fig. 3), I_c, was generally about 90% of that corresponding to the maximum 'm'', $I_{m'}$, or even higher (see Fig. 2a). The difference $I_{m'} - I_c$ decreased when the concentration increased in such a form that for 3 M KOH, the maximum 'm'' was not distinguishable (Table 1).

The total anodic charges measured after long time potentiostatic transients, when the steady state value of current was reached, have been collected in Table 2. An anodic Tafel slope of $0.34\,V\,dec^{-1}$ was obtained for 0.4 M KOH and potentials in the range from

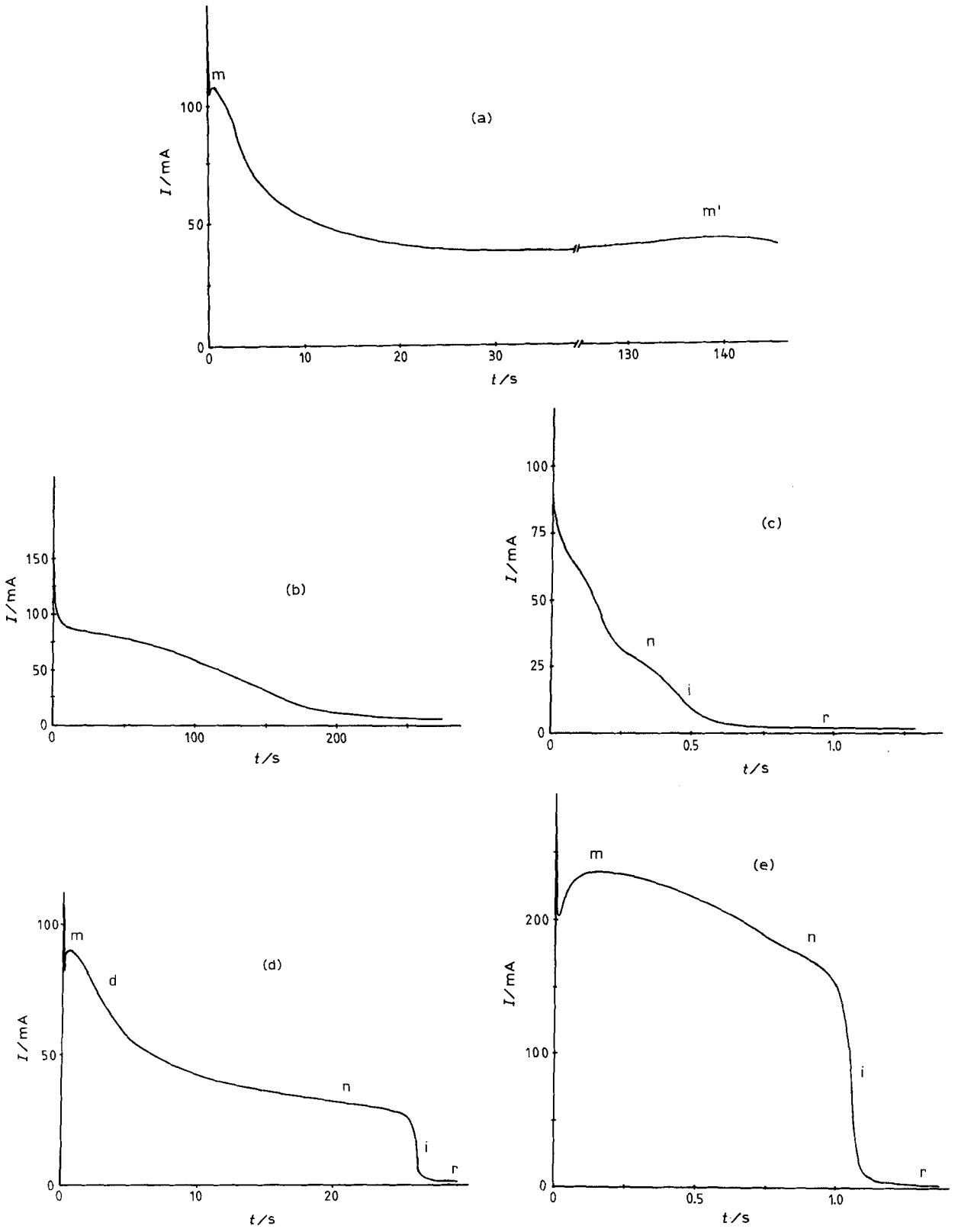

Fig. 2. Potentiostatic transients in quiescent KOH solutions under different conditions: (a) 3.0 M −1100 mV, (b) 1.0 M, −700 mV, (c) 1.0 M, −850 mV, (d) 2.0 M, −1050 mV, and (e) 3.0 M, −800 mV.

−1.05 to −1.2 V (the unique case in which any initial maxima were not found).

3.2. *SEM results*

The state of the metal surface before and after certain potentiostatic transients is shown in Fig. 5a–d. The surface was very rough in all cases and no significant differences when changing the applied potential in the range from −1.2 to −0.7 V were found. Such a roughness, which already appears after the electrode pretreatment (Fig. 5a and b), makes the film thickness determination difficult, because when the film is seen over its section, the film in the ascending part of the craters is also revealed. On the other hand, certain peripheral effect of the electron beam masks the

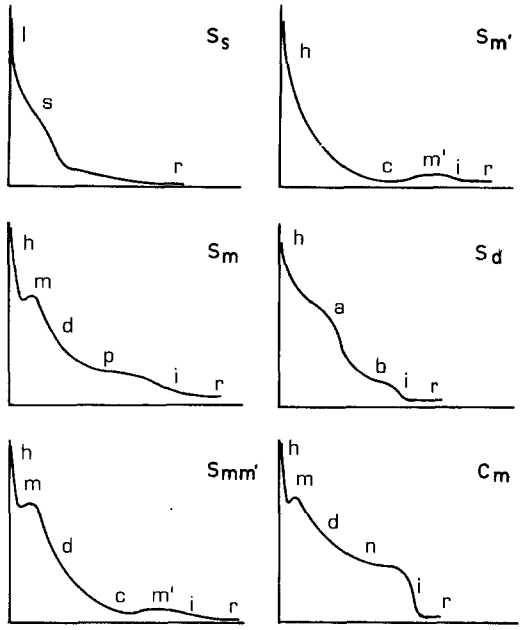

Fig. 3. Schematic drawings of the different types of experimental I–t curves for potentials in the range −1.2 to −0.7 V in quiescent 0.4–4 M KOH solutions.

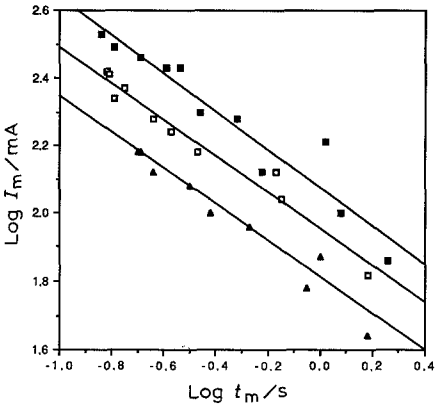

Fig. 4. Log I_m against log t_m plots, I_m and t_m being the current and time corresponding to the maximum 'm' in Fig. 3, for 2 M (▲), 3 M (□) and 4 M (■) KOH solutions.

film/metal interface. According to the corresponding micrographs, i.e. Figs. 5(c) and (d), the film thickness should not be greater than 0.5 μm in the potential range studied (being possibly much lower) and only small changes with potential are envisaged.

3.3. *Coulometric and ICP results*

The coulometric and spectroscopic data concerning the experiments with zinc discs in 2 M KOH are summarized in Tables 3 and 4. In the coulometric experiments, the film thickness was calculated by Faraday's law from the charge associated with film formation, Q_f, calculated as $Q_T - Q_{dis}$, where Q_T is the total charge of the transient and Q_{dis} the charge corresponding to the quantity of film dissolved. The latter was calculated as the product $I_{st}t$, I_{st} being the steady current and t the time of the transient (in steady conditions, the rate of film formation is assumed to be equal to that of dissolution and, therefore, the film thickness is constant). Considering a film density (ZnO porous film) of 4 g cm^{-3} [20] and a roughness factor (σ) of 4, the film thickness should be in the range of 0.095–0.185 μm (Table 3).

The film thickness can be also obtained from the total charge of the transient and the analysis of the zinc content of the working solution (by ICP) after the pretreatment and after the transient. The weight of zinc in the film is determined as $m_f = m_T + m_p - m_d$, where m_T, m_p and m_d are the zinc weights due to the charge of the transient (calculated by Faraday's law), to the pretreatment (cyclic polarization plus cathodic reduction) and to the dissolution process (that is the total zinc dissolved after the pretreatment and the transient), respectively. Considering a porous film density of 4 g cm^{-3} and a roughness factor of 4, film thicknesses in the range 0.14–0.25 μm were obtained (Table 4), which are somewhat greater than those calculated from the charge passed. This can be explained by the film porosity, because in this case, a certain quantity of electrolyte would be trapped inside and as this electrolyte would not be eliminated when stirring in benzene, the analysis of the solution would give lower values of zinc dissolved. Therefore, the most probable film thicknesses are those resulting from the data reported in Table 3.

Table 1. Type of potentiostatic curves found for different potentials and KOH concentrations. (Nomenclature refers to Fig. 4)

E/V ($Hg/HgO/OH^-(C)$)	[KOH]/M				
	0.4	1.0	2.0	3.0	4.0
−1.20	$S_{m'}$	$S_{mm'}$	$S_{mm'}$	$S_{mm'}$*	S_m
−1.15	$S_{m'}$	$S_{mm'}$	$S_{mm'}$	$S_{mm'}$*	S_m
−1.10	$S_{m'}$	$S_{mm'}$	$S_{mm'}$	$S_{mm'}$*	S_m
−1.05	S_s	S_d	C_m	C_m	C_m
−1.00	S_s	S_d	C_m	C_m	C_m
−0.95	S_s	S_d	C_m	C_m	C_m
−0.90	S_s	S_d	C_m	C_m	C_m
−0.85	S_s	S_d	C_m	C_m	C_m
−0.80	S_s	S_d	C_m	C_m	C_m
−0.75	S_s	S_d	S_d	C_m	C_m
−0.70	S_s	S_d†	S_d†	C_m	C_m

* The maximum m' is not practically distinguished
† The second shoulder is not practically observed

*Table 2. Charges (Q) associated with the potentiostatic transients for the different potentials and KOH concentrations**

E/V ($Hg/HgO/OH^-(C)$)	Q/c				
	0.4	1.0	2.0	3.0	4.0
−1.20	1.76	10.9	27	41	43
−1.15	2.20	9.85	20	36	43
−1.10	0.045	9.80	16.0	31.5	49
−1.05	0.022	0.155	1.18	5.72	27.0
−1.00	–	0.075	0.49	1.33	2.08
−0.95	–	0.040	0.30	0.73	1.21
−0.90	0.014	0.027	0.18	0.45	0.82
−0.85	0.010	0.022	0.12	0.27	0.57
−0.80	–	0.022	0.08	0.22	0.44
−0.75	0.007	–	0.05	0.19	0.36
−0.70	–	–	–	0.17	0.30

* Charges measured when the steady value of current was reached.

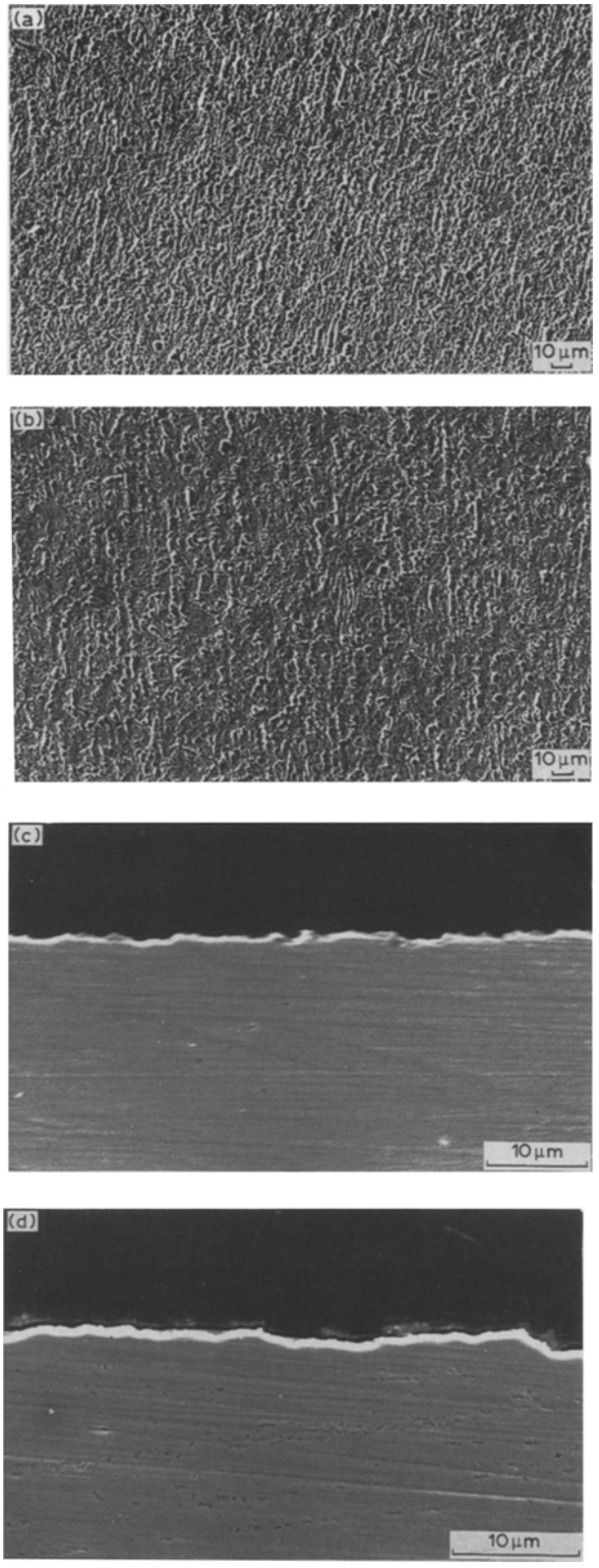

Fig. 5. SEM micrographs of zinc electrodes after the following electrochemical processes in 2 M KOH solutions: (a) electrochemical pretreatment (e.p.); (b) e.p. and -1.05 V; (c) film section for e.p. and -1.05 V and (d) film section for e.p. and -1.2 V.

4. Discussion

4.1. *Film growth test in the initial stages of the transients*

The potentiostatic curves show the existence of an initial maximum ('m' in Figs. 3 and 2d) for KOH concentrations in the range 1.0–4.0 M and potentials of -1.2 V already, which correspond to the linear *I–E* region of the potentiodynamic curves (Fig. 1). The initial maximum in the potentiostatic curves reflects a nucleation like behaviour and therefore, the nucleation and growth of a Zn(II) phase must be inferred. This is in agreement with previous cyclic polarization studies performed in quiescent conditions and the same KOH concentrations [4, 13], in which hydroxide growth was invoked to explain the ohmic behaviour in the region L of Fig. 1. However, the presence of the initial maximum in the potentiostatic curves, instead of a constant current plateau, indicates that the initial stages of the metal oxidation do not take place under ohmic control, or at least it is not the unique factor. In fact, in the potentiodynamic curves, the ohmic control appeared only after the initial charge transfer-controlled dissolution process corresponding to the region X in Fig. 1.

The value of the anodic Tafel slope obtained in the present work, i.e. $0.34\,\mathrm{V\,dec^{-1}}$, differs from that reported in previous work for zinc oxidation to zincate, which was $40\,\mathrm{mV\,dec^{-1}}$ [1, 2, 4, 7]. However, the electrode overvoltages for potentials in the range between -0.7 and -1.2 V are very high, implying that in this region, the mechanism of zinc oxidation is different from that for lower overvoltages. Hampson *et al.* [23] reported a transfer coefficient, also for high overvoltages, from which a Tafel slope of $0.32\,\mathrm{V\,dec^{-1}}$ was calculated [1]. The data reported in Table 2 show that the anodic charge, Q_P, increases with the KOH concentration and decreases when the applied potential is made more positive. A similar situation was found in previous potentiodynamic work [4], in which the anodic charge under the *I–E* curve up to passivation was found to decrease when the sweep rate increased. This was explained by the existence of two processes: the formation of Zn(II) soluble species and film growth by dissolution-precipitation. When the oxidation rate increases, the soluble species have less time to diffuse to the medium and, therefore, less charge is needed to promote metal passivation.

The data treatment to test classical 2D and 3D growths [24] for the region before the maxima 'm' in curves S_m, S_{mm}, and C_m was not successful because the current in the transients does not start from zero. However, as shown in Fig. 6(a) and (b), very good *I* against $t^{-1/2}$ linear relationships were obtained for the current decay after the maxima 'm' in those potentiostatic curves, where the current associated with the maximum, I_m, was much higher than currents associated with regions c, n and p (Fig. 3). This result strongly suggests a 3D diffusion-controlled film growth [25, 26] and agrees with film thickness estimation and Q_P data. In addition, $\ln I_m$ against $\ln t_m$ slopes (Fig. 4) are close to -0.5 and then, the constancy of the product $I_m^2 t_m$ is predicted. $I_m^2 t_m$ is equal to $0.163(nFc^\infty)^2 D$ and $0.260(nFc^\infty)^2 D$ for instantaneous and progressive nucleation, respectively [25, 26],

Table 3. Film thickness estimation from the charge of the transients

E/V	t/s	Q_T/C	I_{st}/mA	Q_{dis}/C	Q_f/C	$\delta\sigma/10^2 nm$	$\delta(\sigma = 4)/10^2 nm$
−1.2	52.0	2.225	36.0	1.872	0.353	7.4	1.85
−1.05	47.6	0.560	6.0	0.286	0.274	5.7	1.44
−0.7	48.0	0.372	4.0	0.192	0.180	3.8	0.94

where c^∞ is the bulk solution concentration of the diffusive species and D is the corresponding diffusion coefficient. The values of D obtained for 2, 3 and 4 M KOH, considering $c^\infty = C_{OH^-}$, where C_{OH^-} is the bulk concentration of OH^-, are about 6×10^{-7} and $4 \times 10^{-7} cm^2 s^{-1}$ for instantaneous and progressive nucleation, respectively. These values are much lower than those normal for diffusion coefficients in liquids, which are about $10^{-5} cm^2 s^{-1}$ and, therefore, it is interpreted that OH^- diffusion is not the film growth-controlling factor. A more reasonable hypothesis is that the process is controlled by the diffusion of zincate.

Barradas and Bosco have reported theoretical *I–t* transients for the metal dissolution as its ions and their diffusion into the solution coupled with a 2D electrocrystallization, the growth of the new phase being determined by the instantaneous concentration of the metal ions at the electrode surface (Model 2 in [27]). The basical difference with the classical electrocrystallization potentiostatic transients is that the current does not begin from zero and an initial current decrease is always found (Fig. 7a). The types of experimental transients obtained in the present work, namely S_s and the initial part of the curves S_m, (the 'hc' region), S_m, $S_{mm'}$, and C_m (the 'hmd' region) are equivalent to those shown in Fig. 7(a). However, such a 2D growth model has been developed for films of the order of monolayers. According to the results of the present work and those of Shan *et al.* [20], the film thickness increases with KOH concentration, being of about 50–100 nm in 1 M KOH and 100–500 nm in 2 M KOH, depending on the conditions. This means 50–500 monolayers in KOH solutions in the range 1–4 M, results which are far from those corresponding to a typical 2D growth. However, the formation of a monolayer has been reported for 0.3 M KOH [5] and a film thickness lower than 20 nm in 0.5 M KOH [20]. All these results strongly suggest that zinc passivation in KOH takes place according to a 3D-modified Barradas and Bosco model, the 3D component increasing with KOH concentration. Such a modification would result from a high rate of zincate formation and low efficiency for film growth.

4.2. *Ohmic control test in the final stages of the transients*

The region 'nir' in curves C_m is equivalent to the potentiostatic transients corresponding to Müller's model on passivation (Fig. 7b) [28–30]. Such a model considers that (a) the new phase grows on nuclei randomly distributed, (b) the film, formed by dissolution-precipitation has a constant thickness during the process, (c) the dissolution and conductivity of the film are negligible and, therefore, the current passes only through non-covered areas and (d) the non-covered areas continuously decrease in size to become small pores in the film. The relationship between the current, I, and time, t, is in this case:

$$t = \tau + A\{[-1/(I_i - I)] + (1/I_i) \times \ln[(I_i - I)/I]\} \quad (1)$$

where I_i is the initial current (Fig. 7b), τ is a measure of the time corresponding to the current plateau and A controls the slope of the current decay. When the reduced variable $x = I/I_i$ is defined, Equation 1 is transformed into:

$$t - \tau = (A/I_i)\{[-1/(1 - x)] + \ln[(1 - x)/x]\} = (A/I_i) f(x) \quad (2)$$

where the factor into brackets has been defined simply as $f(x)$. However, when the pores are small enough, they do not close entirely and the layer grows in depth with the pore area constant. Then, the current–time relationship is

$$t - t_1 = B[I^{-2} - I_1^{-2}] \quad (3)$$

where B is a constant which depends on the pore area and the potential applied. I_1 is the current coresponding to time t_1 during the process of growth in depth.

In order to test the model in the experimental curves obtained in the present work, the $f(x)$ against t and the I^{-2} against t plots were represented for the regions 'ni' and 'ir' of curves C_m (Figs 3, 8 and 9), respectively. Fitting of Equation 2 was performed for curves C_m in which the 'md' region was sufficiently separated from the 'nir' decay, because it was only under such conditions that subtraction of region 'md' from the total curve was possible. As exemplified in Figs 8 and 9, such plots were very satisfactory.

Table 4. Film thickness estimation from the analysis of the zinc content of the working solution. (All these weights are referred to 100 cm^3)

E/V	m_d/mg	Q_T/C	m_T/mg	m_p/mg	m_f/mg	$\delta\sigma/10^2 nm$	$\delta(\sigma = 4)/10^2 nm$
−1.2	1.725	2.225	0.754	1.132	0.161	10.00	2.50
−1.05	1.212	0.50	0.190	1.125	0.103	6.44	1.61
−0.7	1.039	0.372	0.126	1.000	0.087	5.44	1.36

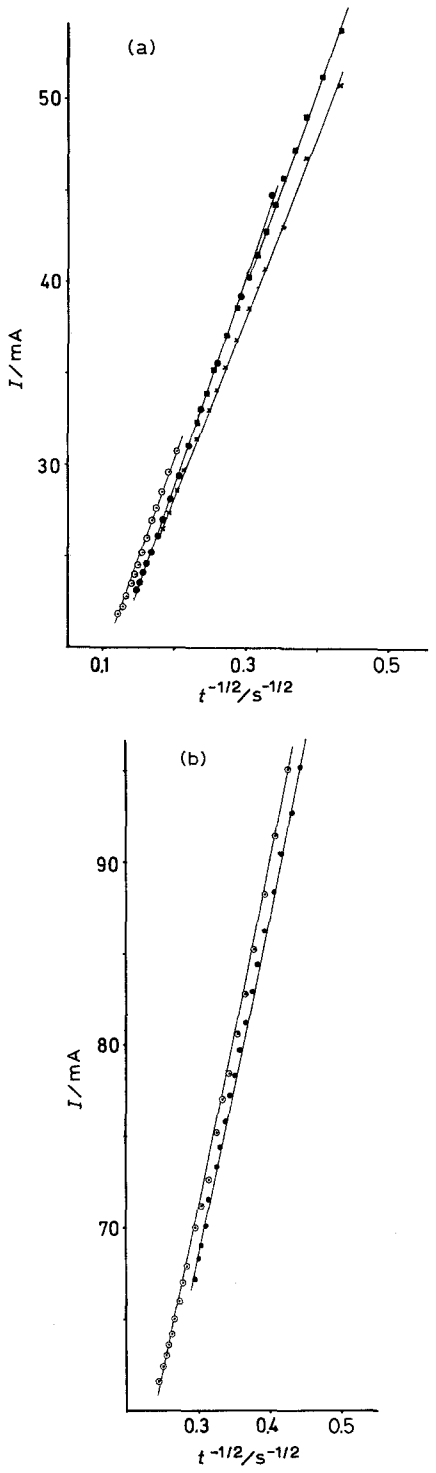

Fig. 6. I against $t^{-1/2}$ plots for the region 'd' of curves S_m, $S_{mn'}$, and C_m in Fig. 3. (a) 2 M KOH, (⊙) −1200, (●) −1150, (×) −1100 and (■) −1050 mV; (b) 3 M KOH, (⊙) −1050 and (●) −1000 mV.

Consequently, it can be concluded that in curves C_m, a diffusion-controlled 3D growth initially takes place and when the resistance of the non-covered areas is sufficiently high, the corresponding growth takes place according to Müller's model. For the most positive potentials in the range studied, the approach between currents corresponding to the maximum 'm' and the region 'n' should be interpreted as due to mixed control by ion diffusion and migration. The passive currents in Fig. 2a–d clearly show that passivation is not complete and a significant current dissolution component exists. This also permits to explain the maximum 'm' in Figs. 2a and 3 simply as due to a change in the roughness of the surface.

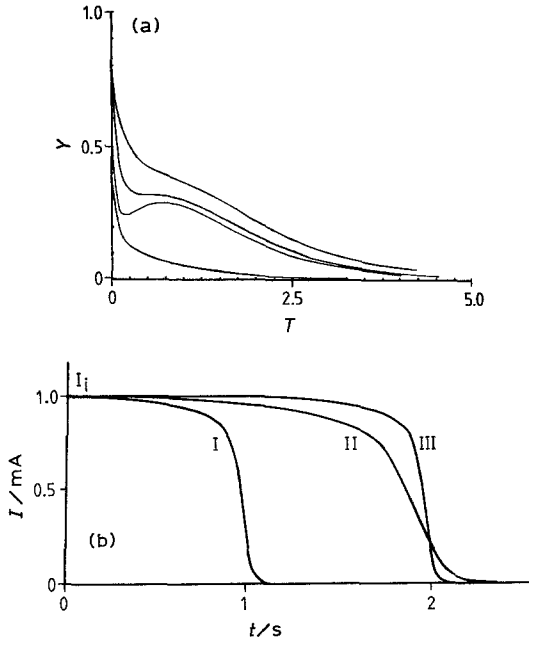

Fig. 7. Schematic current-time curves for the potentiostatic passivation. (a) Non-dimensional current, Y, in front of non-dimensional time, T, corresponding to Model 2 of Barradas and Bosco [27]. The different curves are simulations employing different model parameters, which depend on the potential and on the diffusion coefficient. (b) Müller's model [28, 30] with I_i = 1 mA. Curve I: τ = 1 s, A = 0.02 mA s. Curve II: τ = 2 s, A = 0.06 mA s. Curve III: τ = 2 s, A = 0.02 mA s.

The I^{-2} against t plots were also satisfactory for regions 'ir' of S_d curves (Figs. 2c and 3). For all the KOH concentrations studied, the I–t curves obtained for potentials in the range −1.2 to −1.1 V do not exhibit the sharp current decay which is found in the curves C_m ('nir' in Figs. 2d and 3) and instead, a very slow but sigmoidal current decrease is found. This validates the existence of a significant dissolution of the film formed and only when the film is sufficiently thick, does ohmic control appear.

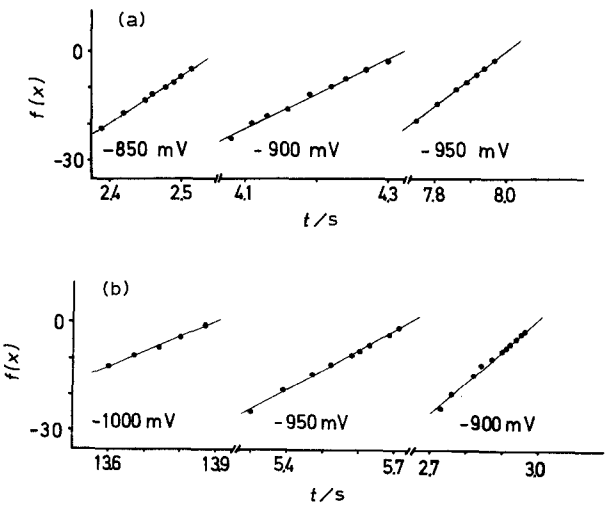

Fig. 8. $f(x)$ against t plots for region 'ni' in curves of C_m type, according to Equation (2). (a) 4 M KOH. (b) 3 M KOH.

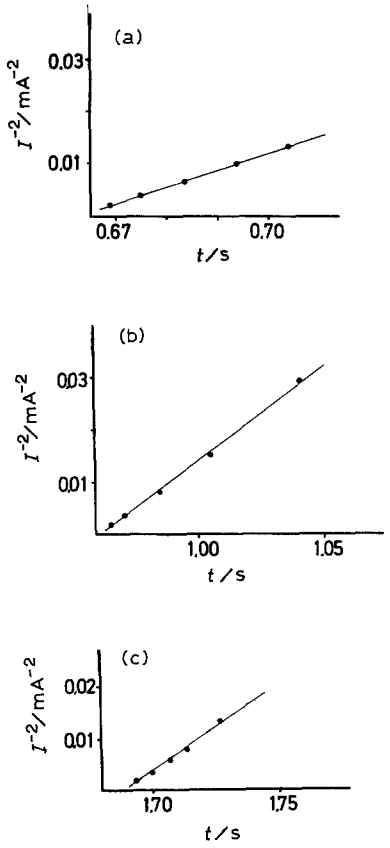

Fig. 9. I^{-2} against t plots for region ir in curves of C_m type, according to Equation 3. 2 M KOH solutions. (a) −0.8 V. (b) −0.85 V. (c) −0.9 V.

5. Conclusions

Two different zones are discerned in the potentiostatic passivation of zinc in KOH solutions in the range 0.4–4 M. The first, in the initial stages of the transient, can be explained by a model of direct oxidation to zincate, in which part of these ions diffuse into the solution and the rest react with OH^- to form the anodic film. The growth tends to a 2D type at low KOH concentrations, but evolves to a 3D type when the KOH concentration increases. The results are compatible with a porous film whose thickness increases with KOH concentration. In such a first zone, when the film starts to grow, the process is diffusion-controlled. The second zone, appearing in the final stages of the transients, is attributed to a film growth according to Müller's model. In this case, the process is controlled by ion migration through the pores in the film when the latter is sufficiently thick. The efficiency for film formation is low in all the cases, this explaining the relatively high values of the passive currents.

Acknowledgements

The authors gratefully acknowledge the 'Servei Científico-Tènic de la Universitat de Barcelona' for the facilities in the SEM observation and the ICP analysis.

References

[1] J. O'M. Bockris, Z. Nagy and A. Damjanovic, *J. Electrochem. Soc.* **119** (1972) 285.
[2] J. Hendrikx, A. van der Putten, W. Visscher and E. Barendrecht, *Electrochim. Acta* **29** (1984) 81.
[3] J. Hendrikx, W. Visscher and E. Barendrecht, *ibid.* **30** (1985) 999.
[4] P. L. Cabot, M. Corts, F. Centellas, J. A. Garrido and E. Prez, *J. Electroanal. Chem.* **201** (1986) 85.
[5] R. D. Armstrong and G. M. Bulman, *ibid.* **25** (1970) 121.
[6] R. D. Armstrong and M. F. Bell, *ibid.* **55** (1974) 201.
[7] Y. C. Chang and G. Prentice, *J. Electrochem. Soc.* **132** (1985) 375.
[8] *Idem, ibid.* **136** (1989) 3398.
[9] M. C. H. McKubre and D. D. Macdonald, *ibid.* **128** (1981) 524.
[10] L. M. Baugh and A. Higginson, *Electrochim. Acta* **30** (1985) 1163.
[11] R. W. Powers and M. W. Breiter, *J. Electrochem. Soc.* **116** (1969) 719.
[12] M. W. Breiter, *Electrochim. Acta* **15** (1970) 1297.
[13] P. L. Cabot, M. Cortés, E. Gómez and E. Vallés, *J. Electroanal. Chem.* **247** (1988) 323.
[14] M. Eisenberg, H. F. Bauman and D. M. Brettner, *J. Electrochem. Soc.* **108** (1961) 909.
[15] M. B. Liu, G. M. Cook and N. P. Yao, *ibid.* **128** (1981) 1663.
[16] M. N. Hull and J. E. Toni, *Trans. Faraday Soc.* **67** (1971) 1128.
[17] L. M. Baugh and A. R. Baikie, *Electrochim. Acta* **30** (1985) 1173.
[18] R. D. Armstrong, G. M. Bulman and H. R. Thirsk, *J. Electroanal. Chem.* **22** (1969) 55.
[19] H. Kaesche, *Electrochim. Acta* **9** (1964) 383.
[20] X. Shan, D. Ren, P. Scholl and G. Prentice, *J. Electrochem. Soc.* **136** (1989) 3594.
[21] B. Aurian-Blajeni and M. Tomkiewicz, *ibid.* **132** (1985) 1511.
[22] *Idem, ibid.* **133** (1986) 1766.
[23] W. A. Hampson, G. A. Herdman and R. Taylor, *J. Electroanal. Chem.* **25** (1970) 9.
[24] R. Greef, R. Peat, L. M. Peter, D. Pletcher and J. Robinson, 'Instrumental Methods in Electrochemistry', Ellis Horwood, London (1985).
[25] B. R. Scharifker and G. J. Hills, *Electrochim. Acta* **28** (1983) 879.
[26] E. Bosco and S. K. Rangarajan, *J. Electroanal. Chem.* **134** (1981) 213.
[27] R. Barradas and E. Bosco, *Electrochim. Acta* **31** (1986) 949.
[28] W. M. Müller, *Trans. Faraday Soc.* **27** (1931) 737.
[29] L. Stephenson and J. H. Bartlett, *J. Electrochem. Soc.* **101** (1954) 571.
[30] R. S. Cooper, *J. Electrochem. Soc.* **103** (1956) 307.